

Two-dimensional anisotropic Dirac materials PtN_4C_2 and $\text{Pt}_2\text{N}_8\text{C}_6$ with quantum spin and valley Hall effects

Jingping Dong^{1,*}, Chuhan Wang^{1,*}, Xinlei Zhao¹, Miao Gao², Xun-Wang Yan^{3,†}, Fengjie Ma^{1,‡} and Zhong-Yi Lu⁴

¹The Center for Advanced Quantum Studies and Department of Physics, Beijing Normal University, Beijing 100875, China

²Department of Physics, School of Physical Science and Technology, Ningbo University, Zhejiang 315211, China

³College of Physics and Engineering, Qufu Normal University, Shandong 273165, China and

⁴Department of Physics, Renmin University of China, Beijing 100872, China
(Dated: July 11, 2022)

We propose two novel two-dimensional topological Dirac materials, planar PtN_4C_2 and $\text{Pt}_2\text{N}_8\text{C}_6$, which exhibit graphene-like electronic structures with linearly dispersive Dirac-cone states exactly at the Fermi level. Moreover, the Dirac cone is anisotropic, resulting in anisotropic Fermi velocities and making it possible to realize orientation-dependent quantum devices. Using the first-principles electronic structure calculations, we have systemically studied the structural, electronic, and topological properties. We find that spin-orbit coupling opens a sizable topological band gap so that the materials can be classified as quantum spin Hall insulators as well as quantum valley Hall insulators. Helical edge states that reside in the insulating band gap connecting the bulk conduction and valence bands are observed. Our work not only expands the Dirac cone material family, but also provides a new avenue to searching for more two-dimensional topological quantum spin and valley Hall insulators.

I. INTRODUCTION

Two-dimensional topological Dirac materials ignited by graphene have attracted tremendous interests in the past decade, owing to their unique properties in the reduced dimension and promising prospects for both fundamental research and applications^{1,2}. These materials are characterized by a linear energy dispersion at the Fermi energy, exhibiting many novel phenomena and exotic physics, such as massless fermions, fractional quantum Hall effect, and quantum spin Hall effect³⁻¹². However, due to the various requirements associated with the crystal symmetries and orbital interactions, the available two-dimensional systems hosting Dirac cones and vanishing density of states right at the Fermi level are very rare¹¹⁻²². It is still a very challenging task to searching for more novel two-dimensional Dirac materials, in which materials with topologically nontrivial properties are even rarer.

When spin-orbit coupling is included in two-dimensional Dirac materials, a global band gap opens and the materials are turned into two-dimensional topological quantum spin Hall insulators with metallic helical edge states residing in the insulating bulk gap^{12,23,24}. Due to time-reversal symmetry, these helical edge states come in Kramers' pairs, so that electrons with opposite spins propagate in opposite directions. In addition, the helical edge states are protected from back-scattering, giving rise to a symmetry-protected topological phase with a quantised spin Hall conductance. However, a rather weak intrinsic spin-orbit coupling often limits the experimental realization of such a two-dimensional topological Dirac system. A sizable spin-orbit coupling is thus very crucial for the realization of a two-dimensional quantum spin Hall insulator^{12,25}. For example, the observation of quantum spin Hall effect in graphene has not been

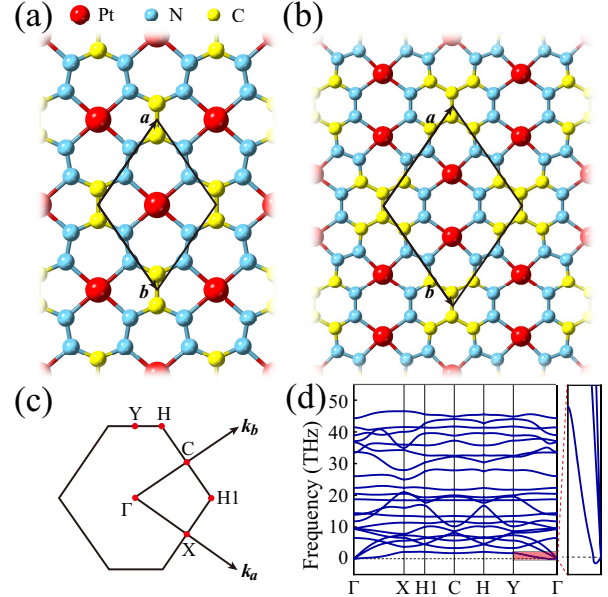


FIG. 1. (a) Atomic structure of monolayer PtN_4C_2 , in which the red, blue, and yellow balls represent Pt, N, and C atoms, respectively. The black solid line illustrates the primitive cell. (b) Atomic structure of monolayer $\text{Pt}_2\text{N}_8\text{C}_6$. (c) The corresponding Brillouin zone of PtN_4C_2 with high-symmetry k-points labeled. (d) Phonon spectrum of PtN_4C_2 with a zoomed-in graph in range of -0.2 to 2 THz.

experimental confirmed yet, due to its negligible spin-orbit coupling and rather tiny splitting energy gap which make it easy for electrons to thermalize to the conduction bands²⁶.

Recently, a novel class of single-atom-thick two-dimensional transition metal carbonitrides, including CrN_4C_2 , CoN_4C_2 , $\text{CoN}_4\text{C}_{10}$, $\text{Co}_2\text{N}_8\text{C}_6$, and $\text{Co}_2\text{N}_6\text{C}_6$,

has been proposed based on the first-principles electronic structure calculations^{27–29}. In comparison with the prototype graphene, transition metal elements are incorporated into the new planar graphene-like structures, resulting in richer electronic properties, such as flat bands, Van-Hove singularity, and intrinsic two-dimensional ferromagnetism^{27–29}. Moreover, due to the introduction of heavy-metal atoms that have much stronger spin-orbit coupling, more prominent topological properties may be expected in this class of materials.

In this paper, based on the first-principles electronic structure calculations, we propose two new types of two-dimensional planar materials, PtN₄C₂ and Pt₂N₈C₆ (Fig. 1), which share the similar structure with CoN₄C₂ and Co₂N₈C₆ respectively^{27,28}, exhibiting a significant quantum spin Hall effect and holding a great promise for experimental realization. In the absence of spin-orbit coupling, they are perfect gapless Dirac semimetals. However, unlike graphene in which the Dirac points locate at the particularly symmetric K and K' points on the Brillouin zone boundary, the Dirac nodes of PtN₄C₂ and Pt₂N₈C₆ locate at a general k-point along the Y–Γ high-symmetry path, away from the K/K' points. This is due to the structural distortion in comparison with the ideal honeycomb lattice. Furthermore, the linear band dispersions of PtN₄C₂ and Pt₂N₈C₆ around the Dirac nodes are anisotropic, different from the isotropic Dirac cones with the vertical axes of graphene¹¹, making them suitable to realize orientation-dependent quantum devices. Once spin-orbit coupling is considered, sizable band gaps, ~ 10 meV and 40 meV, are opened for PtN₄C₂ and Pt₂N₈C₆ respectively, and the materials are converted into quantum spin Hall insulators with topological index $\mathbb{Z}_2=1$. Topological nontrivial properties, including the Berry curvature, spin-Hall conductivity, and helical edge states are systematically studied. These quantum phenomena should be observable in experiment, especially for Pt₂N₈C₆ in which the gap is sufficiently large for practical applications at room temperature. Since PtN₄C₂ and Pt₂N₈C₆ monolayers are very similar, here we take PtN₄C₂ as an example to illustrate their electronic and topological properties. The results of Pt₂N₈C₆ are presented in the Supplementary Materials³⁰.

II. METHODS

In our calculations, the plane-wave basis based method and Quantum-ESPRESSO software package were used^{31,32}. We adopted the generalized gradient approximation (GGA) of Perdew-Burke-Ernzerhof formula for the exchange-correlation potentials in the electronic structure simulations³³. The ultrasoft pseudopotentials were employed to model the electron-ion interactions³⁴. A slab geometry was applied, where we added a vacuum space of ~ 20 Å in the *z* direction to eliminate the periodic effect. The mesh of k-points grid used for sampling the Brillouin zone was 24×24×1, and the Marzari-

Vanderbilt broadening technique was adopted³⁵. After full convergence tests, the kinetic energy cutoff for wavefunctions and charge densities were chosen to be 90 and 720 Ry, respectively. During the simulations, all structural geometries were fully optimized to achieve the minimum energy. Phonon band dispersions were calculated by using density functional perturbation theory based on the PHONOPY program³⁶. The edge states were studied using tight-binding methods by the combination of Wannier90³⁷ and WannierTools³⁸ software packages.

III. STRUCTURAL AND ELECTRONIC PROPERTIES

The atomic structure of monolayer PtN₄C₂ belongs to the *Cmmm* space group with No. 65, which is affiliated to the *D_{2h}* point group symmetry, as shown in Fig. 1(a). There are totally one Pt, four N, and two C atoms in the primitive cell (the solid black rhombus), in which the Pt atom is tetra-coordinated by four N atoms, forming PtN₄ complexes connected by the C atoms. All three kinds of atoms in PtN₄C₂ are coplanar after structural relaxation. The optimized lattice parameters of PtN₄C₂ are $a = b = 4.789$ Å and the angle between the two basis vectors $\alpha = 110.45^\circ$. Figure 1(c) sketches the corresponding Brillouin zone of PtN₄C₂ with the high symmetry points labeled, which is slightly distorted from the perfect honeycomb structure. The angle between the two reciprocal vectors is no longer 60°, and hence, the high symmetry k-points *H* and *X* become inequivalent *H*1 and *Y*, respectively. The dynamical stability of PtN₄C₂ can be demonstrated by calculating its phonon dispersion curve. As shown in Fig. 1(d), no considerable imaginary frequency appears in the entire Brillouin zone, indicating that the PtN₄C₂ monolayer is dynamically stable. Note that there is a tiny spoon-shaped pocket near the Γ point as shown in the zoomed-in graph, which is due to the difficulty of achieving numerical convergence for the flexural phonon branch. It is a common issue in the first-principles electronic structure calculations on 2D materials and does not imply instability^{39,40}.

Figure 2 shows the calculated electronic band structure of PtN₄C₂. Similar to graphene, PtN₄C₂ is a perfect Dirac semimetal with vanishing density of states at the Fermi level in the absence of spin-orbit coupling, as shown in Fig. 2(a). By projecting the band structures onto different atomic orbitals, the Dirac node is found to mainly consist of the N-*p*, C-*p*, and Pt-*d* states. More specifically, the N-*p_z* and C-*p_z* form a π network together with the Pt *d_{xz}* and *d_{yz}* orbitals in the vicinity of the Fermi level, as shown in Fig. 2(b). However, different from those of graphene, the linearly dispersive Dirac nodes of PtN₄C₂ do not locate at the particularly high-symmetric K or K' points on the Brillouin zone boundary. They locate at a general k-point in the high-symmetry line Y–Γ, as displayed in Fig. 2(c). Therefore, there are two Dirac nodes (in the high-symmetry Y–Γ and -

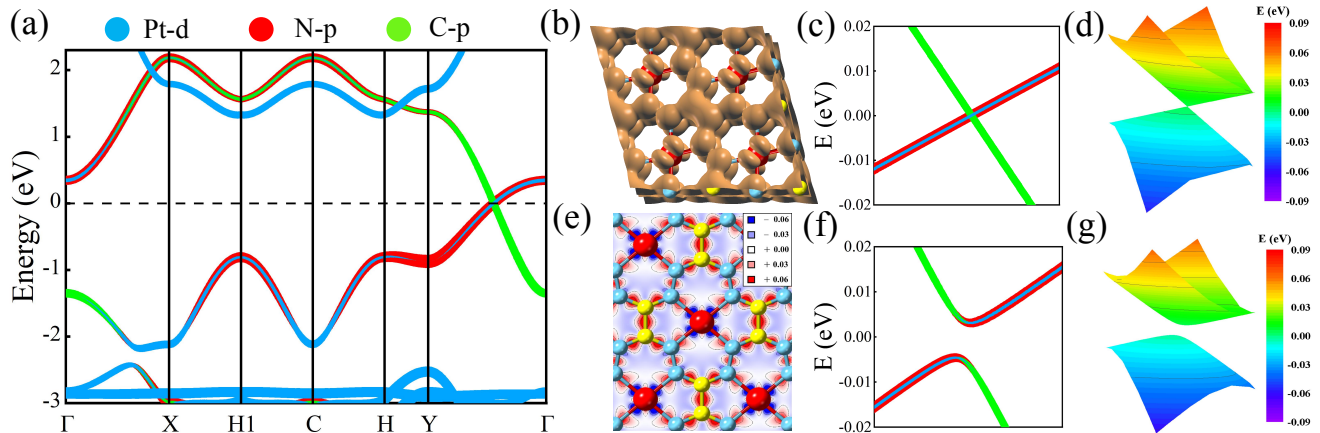


FIG. 2. (a) Orbital-resolved band structure of monolayer PtN_4C_2 without spin-orbit coupling. The black dashed line represents the Fermi level. (b) The charge density distributions from the wavefunctions of the lowest conduction and highest valence bands at the Dirac point. A π network is formed by the $\text{N-}p_z$ and $\text{C-}p_z$ together with the Pt d_{xz} and d_{yz} orbitals. Here the isovalue is set to 0.0035 e/bohr^3 . (c) and (d) give the zoomed-in view of the area around the Dirac point with orbital projections and the corresponding three-dimensional energy dispersion of bands without spin-orbit coupling. (e) The distribution of differential charge density. The red and blue in the isosurface views represent the accumulation and depletion of electrons in units of e/bohr^3 , respectively. (f) and (g) show the zoomed-in view of the area around the Dirac point with orbital projections and the corresponding three-dimensional energy dispersion of bands with spin-orbit coupling.

$Y-\Gamma$ paths) within the first Brillouin zone, as shown in Fig. 2(d), which illustrates the energy dispersion of highest valence and lowest conduction bands of PtN_4C_2 as a function of k . The two bulk bands touch only at the Dirac points, forming the two Dirac cones within the first Brillouin zone. Moreover, the Dirac cones are tilted compared with that of graphene. This is due to the reduced lattice spatial symmetry D_{2h} of PtN_4C_2 , in comparison with the D_{6h} symmetry of graphene. The distortion of primitive unit cell from an ideal honeycomb lattice causes the shift of the Dirac cones in the distorted first Brillouin zone with lower spatial symmetry⁴¹. The linear band dispersions around the Dirac cones are therefore anisotropic, resulting in anisotropic Fermi velocities and making them possible to realize orientation-dependent quantum devices.

We further calculated the differential charge density of PtN_4C_2 to illustrate the internal bonding conditions and the charge transfer, as shown in Fig. 2(e). The red/blue colours mark an increase/decrease of the charge density. There is significant charge accumulation between the C–N, N–N, and C–C atoms, indicating that covalent bonds are formed between these atoms. The charge depletion happens mostly around the Pt atoms, supporting the transfer of electrons to the neighbor N atoms in the local PtN_4 complex. Therefore, an ionic bond is formed between Pt and N atoms.

Once spin-orbit coupling is introduced in calculations, an energy gap is opened at the Dirac point, turning the linear band dispersions into quadratic ones, as shown in Fig. 2(f). Since Pt belongs to a heavy transition-metal element, a larger energy gap of $\sim 10 \text{ meV}$ is observed, in comparison with that of graphene on the or-

der of μeV ²⁶. The splitting gap is experimentally visible and is capable of hosting novel quantum spin Hall states. Figure 2(g) shows the three-dimensional energy dispersion of highest valence and lowest conduction bands of PtN_4C_2 with spin-orbit coupling. Compared to the one without spin-orbit coupling (Fig. 2(c)), the quadratic feature with an open energy gap is evident. PtN_4C_2 is therefore very likely to be a quantum spin Hall insulator, possessing symmetry-protected helical metallic edge states that have myriad potential applications in electronics and spintronics.

IV. TOPOLOGICAL PROPERTIES

Based on the DFT band structure with spin-orbit coupling, we construct a tight-bind Hamiltonian of PtN_4C_2 in the basis of maximally localized wannier functions through the Wannier90 program^{37,42}. The topological properties of PtN_4C_2 can then be studied with WannierTools software package based on the Green's function method^{38,43}.

As shown in Fig. 3(a), the band structure given by the means of maximally localized wannier functions agrees very well with the one given by the DFT calculations, in which Pt- s, p, d , N- s, p , and C- s, p orbitals are adopted as the projection orbitals. To further confirm the topological non-trivialness of PtN_4C_2 , we have calculated the topological \mathbb{Z}_2 invariant. The method of Wannier charge center evolution in half Brillouin zone is adopted^{44,45}. As shown in Fig. 3(b), it is clear from the figure that the Wannier charge center evolution curves cut an arbitrary horizontal reference line odd times, indicating a value

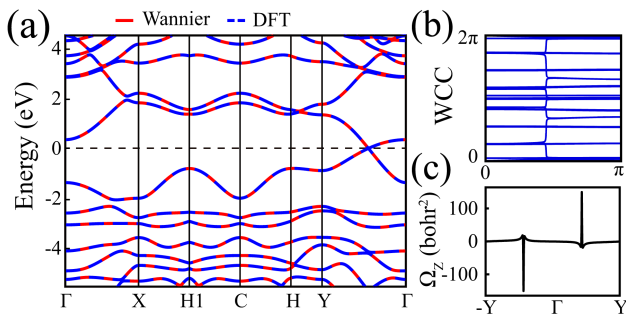


FIG. 3. (a) The comparison of the band structure of PtN_4C_2 between the Wannier tight-binding Hamiltonian (red solid lines) and the DFT calculations (blue dashed lines). Spin-orbit coupling is included. (b) The evolution of Wannier charge center (WCC) curves in half Brillouin zone for calculating the \mathbb{Z}_2 invariant. (c) The Berry curvature along the high-symmetry $-\tilde{Y}-\tilde{\Gamma}-\tilde{Y}$ path in the Brillouin zone.

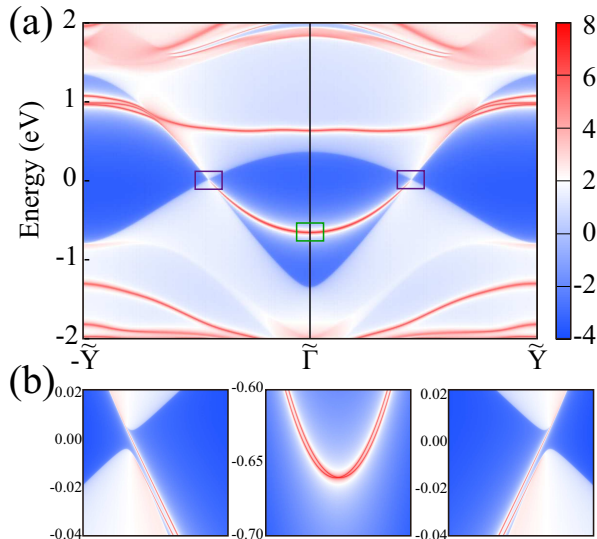


FIG. 4. (a) The helical edge states and bulk band structure of PtN_4C_2 projected along the (100) direction. (b) Zoomed-in view of the areas highlighted by the boxes that surround the projected Dirac nodes and the $\tilde{\Gamma}$ point respectively in (a).

of $\mathbb{Z}_2 = 1$. Thus the gapped PtN_4C_2 with spin-orbit coupling is indeed a two-dimensional \mathbb{Z}_2 topological insulator. Meanwhile, from Fig. 3(c), the distribution of Berry curvature shows that the Berry phases around the two Dirac points within the Brillouin zone are opposite, as determined by the time-reversal symmetry, indicating that PtN_4C_2 is also a quantum valley Hall insulator^{46–49}.

We further investigate the helical edge states of PtN_4C_2 projected along the (100) direction, whose band dispersions are given in Fig. 4(a). The topological non-

trivial edge states are visible, which thread across the bulk band gap and connect the bulk conduction and valence bands of PtN_4C_2 at the two projected Dirac points in the Brillouin zone along the high-symmetry line $-\tilde{Y}-\tilde{\Gamma}-\tilde{Y}$. Figure 4(b) gives the zoomed-in view of the areas highlighted by the boxes that surround the projected Dirac nodes and the $\tilde{\Gamma}$ point respectively in Fig. 4(a). There are two edge states separately emerging from the bulk conduction/valence bands of one Dirac node and merging into the valence/conduction continuum of the other Dirac node within the Brillouin zone. They cross each other and form a single Dirac cone inside the bulk gap at the $\tilde{\Gamma}$ point, protected by time-reversal symmetry which induces the Kramers degeneracy, as shown in middle panel of Fig. 4(b). The spin-momenta of these states are locked and protected from backscattering. This behavior is the main characteristic of the quantum spin Hall effect, which makes PtN_4C_2 promising for novel electronic and spintronic applications^{23,24}.

V. SUMMARY

In summary, based on symmetry analysis and the first-principles electronic structure calculations, we predict that PtN_4C_2 and $\text{Pt}_2\text{N}_8\text{C}_6$ are two perfect two-dimensional topological Dirac materials. Due to the lattice distortion from ideal honeycomb structure, linear anisotropic band dispersions around the Dirac cones are found, making both compounds a promising platform to realize orientation-dependent quantum devices. With spin-orbit coupling included, a sizable topological non-trivial band gap opens, and the two-dimensional materials transform into a quantum spin Hall insulator as well as a quantum valley Hall insulator, characterized by an odd \mathbb{Z}_2 , topological helical edge states, and symmetry-protected opposite Berry curvatures. Our work not only expands the Dirac cone material family, but also provides a new avenue to searching for more two-dimensional topological quantum spin and valley Hall insulators.

Note added: After preparation of this manuscript, we noticed a paper recently published in PRB⁵⁰, proposing a PtN_4 -embedded graphene $\text{PtN}_4\text{C}_{10}$ that shares similar structural recipes with the PtN_4C_2 and $\text{Pt}_2\text{N}_8\text{C}_6$ systems discussed here, also found to be a two-dimensional quantum Hall insulator.

VI. ACKNOWLEDGMENTS

This work was financially supported by the National Natural Science Foundation of China under Grants Nos. 12074040, 11974207, and 11974194.

* These authors contributed equally to this work.

† yanxunwang@163.com

- ‡ fengjie.ma@bnu.edu.cn
- ¹ J. Wang, S. Deng, Z. Liu, and Z. Liu, *National Science Review* **2**, 22 (2015).
 - ² K. S. Novoselov, A. K. Geim, S. V. Morozov, D. Jiang, Y. Zhang, S. V. Dubonos, I. V. Grigorieva, and A. A. Firsov, *Science* **306**, 666 (2004).
 - ³ Y. Zhang, Y.-W. Tan, H. L. Stormer, and P. Kim, *Nature* **438**, 201 (2005).
 - ⁴ K. I. Bolotin, F. Ghahari, M. D. Shulman, H. L. Stormer, and P. Kim, *Nature* **462**, 196 (2009).
 - ⁵ X. Du, I. Skachko, F. Duerr, A. Luican, and E. Y. Andrei, *Nature* **462**, 192 (2009).
 - ⁶ C. R. Dean, L. Wang, P. Maher, C. Forsythe, F. Ghahari, Y. Gao, J. Katoch, M. Ishigami, P. Moon, M. Koshino, T. Taniguchi, K. Watanabe, K. L. Shepard, J. Hone, and P. Kim, *Nature* **497**, 598 (2013).
 - ⁷ L. A. Ponomarenko, R. V. Gorbachev, G. L. Yu, D. C. Elias, R. Jalil, A. A. Patel, A. Mishchenko, A. S. Mayorov, C. R. Woods, J. R. Wallbank, M. Mucha-Kruczynski, B. A. Piot, M. Potemski, I. V. Grigorieva, K. S. Novoselov, F. Guinea, V. I. Fal'ko, and A. K. Geim, *Nature* **497**, 594 (2013).
 - ⁸ B. Hunt, J. D. Sanchez-Yamagishi, A. F. Young, M. Yankowitz, B. J. LeRoy, K. Watanabe, T. Taniguchi, P. Moon, M. Koshino, P. Jarillo-Herrero, and R. C. Ashoori, *Science* **340**, 1427 (2013).
 - ⁹ A. H. Castro Neto, F. Guinea, N. M. R. Peres, K. S. Novoselov, and A. K. Geim, *Rev. Mod. Phys.* **81**, 109 (2009).
 - ¹⁰ N. O. Weiss, H. Zhou, L. Liao, Y. Liu, S. Jiang, Y. Huang, and X. Duan, *Advanced Materials* **24**, 5782 (2012).
 - ¹¹ K. S. Novoselov, A. K. Geim, S. V. Morozov, D. Jiang, M. I. Katsnelson, I. V. Grigorieva, S. V. Dubonos, and A. A. Firsov, *Nature* **438**, 197 (2005).
 - ¹² C.-C. Liu, W. Feng, and Y. Yao, *Phys. Rev. Lett.* **107**, 076802 (2011).
 - ¹³ S. Cahangirov, M. Topsakal, E. Aktürk, H. Şahin, and S. Ciraci, *Phys. Rev. Lett.* **102**, 236804 (2009).
 - ¹⁴ D. Malko, C. Neiss, F. Viñes, and A. Görling, *Phys. Rev. Lett.* **108**, 086804 (2012).
 - ¹⁵ H. Huang, W. Duan, and Z. Liu, *New Journal of Physics* **15**, 023004 (2013).
 - ¹⁶ Y. Ma, Y. Dai, X. Li, Q. Sun, and B. Huang, *Carbon* **73**, 382 (2014).
 - ¹⁷ L.-C. Xu, R.-Z. Wang, M.-S. Miao, X.-L. Wei, Y.-P. Chen, H. Yan, W.-M. Lau, L.-M. Liu, and Y.-M. Ma, *Nanoscale* **6**, 1113 (2014).
 - ¹⁸ F. Ouyang, S. Peng, Z. Liu, and Z. Liu, *ACS Nano* **5**, 4023 (2011).
 - ¹⁹ X.-F. Zhou, X. Dong, A. R. Oganov, Q. Zhu, Y. Tian, and H.-T. Wang, *Phys. Rev. Lett.* **112**, 085502 (2014).
 - ²⁰ W. Li, M. Guo, G. Zhang, and Y.-W. Zhang, *Phys. Rev. B* **89**, 205402 (2014).
 - ²¹ Z. F. Wang, Z. Liu, and F. Liu, *Nature Communications* **4**, 1471 (2013).
 - ²² K. K. Gomes, W. Mar, W. Ko, F. Guinea, and H. C. Manoharan, *Nature* **483**, 306 (2012).
 - ²³ M. Z. Hasan and C. L. Kane, *Rev. Mod. Phys.* **82**, 3045 (2010).
 - ²⁴ X.-L. Qi and S.-C. Zhang, *Rev. Mod. Phys.* **83**, 1057 (2011).
 - ²⁵ W.-F. Tsai, C.-Y. Huang, T.-R. Chang, H. Lin, H.-T. Jeng, and A. Bansil, *Nature Communications* **4**, 1500 (2013).
 - ²⁶ Y. Yao, F. Ye, X.-L. Qi, S.-C. Zhang, and Z. Fang, *Phys. Rev. B* **75**, 041401(R) (2007).
 - ²⁷ D. Liu, S. Zhang, M. Gao, and X.-W. Yan, *Phys. Rev. B* **103**, 125407 (2021).
 - ²⁸ D. Liu, P. Feng, M. Gao, and X.-W. Yan, *Phys. Rev. B* **103**, 155411 (2021).
 - ²⁹ D. Liu, S. Zhang, M. Gao, X.-W. Yan, and Z. Y. Xie, *Applied Physics Letters* **118**, 223104 (2021).
 - ³⁰ The results of Pt₂N₈C₆ are listed in the Supplementary Materials.
 - ³¹ P. Giannozzi, S. Baroni, N. Bonini, M. Calandra, R. Car, C. Cavazzoni, D. Ceresoli, G. L. Chiarotti, M. Cococcioni, I. Dabo, A. D. Corso, S. de Gironcoli, S. Fabris, G. Fratesi, R. Gebauer, U. Gerstmann, C. Gougoussis, A. Kokalj, M. Lazzeri, L. Martin-Samos, N. Marzari, F. Mauri, R. Mazzarello, S. Paolini, A. Pasquarello, L. Paulatto, C. Sbraccia, S. Scandolo, G. Sclauzero, A. P. Seitsonen, A. Smogunov, P. Umari, and R. M. Wentzcovitch, *Journal of Physics: Condensed Matter* **21**, 395502 (2009).
 - ³² P. Giannozzi, O. Andreussi, T. Brumme, O. Bunau, M. B. Nardelli, M. Calandra, R. Car, C. Cavazzoni, D. Ceresoli, M. Cococcioni, N. Colonna, I. Carnimeo, A. D. Corso, S. de Gironcoli, P. Delugas, R. A. DiStasio, A. Ferretti, A. Floris, G. Fratesi, G. Fugallo, R. Gebauer, U. Gerstmann, F. Giustino, T. Gorni, J. Jia, M. Kawamura, H.-Y. Ko, A. Kokalj, E. Küçükbenli, M. Lazzeri, M. Marsili, N. Marzari, F. Mauri, N. L. Nguyen, H.-V. Nguyen, A. O. de-la Roza, L. Paulatto, S. Poncé, D. Rocca, R. Sabatini, B. Santra, M. Schlipf, A. P. Seitsonen, A. Smogunov, I. Timrov, T. Thonhauser, P. Umari, N. Vast, X. Wu, and S. Baroni, *Journal of Physics: Condensed Matter* **29**, 465901 (2017).
 - ³³ J. P. Perdew, K. Burke, and M. Ernzerhof, *Phys. Rev. Lett.* **77**, 3865 (1996).
 - ³⁴ D. Vanderbilt, *Phys. Rev. B* **41**, 7892(R) (1990).
 - ³⁵ N. Marzari, D. Vanderbilt, A. De Vita, and M. C. Payne, *Phys. Rev. Lett.* **82**, 3296 (1999).
 - ³⁶ A. Togo and I. Tanaka, *Scripta Materialia* **108**, 1 (2015).
 - ³⁷ A. A. Mostofi, J. R. Yates, Y.-S. Lee, I. Souza, D. Vanderbilt, and N. Marzari, *Computer Physics Communications* **178**, 685 (2008).
 - ³⁸ Q. Wu, S. Zhang, H.-F. Song, M. Troyer, and A. A. Soluyanov, *Computer Physics Communications* **224**, 405 (2018).
 - ³⁹ V. Zólyomi, N. D. Drummond, and V. I. Fal'ko, *Phys. Rev. B* **89**, 205416 (2014).
 - ⁴⁰ H. D. Tran, M. Amsler, S. Botti, M. A. L. Marques, and S. Goedecker, *The Journal of Chemical Physics* **140**, 124708 (2014).
 - ⁴¹ Z. Wang, X.-F. Zhou, X. Zhang, Q. Zhu, H. Dong, M. Zhao, and A. R. Oganov, *Nano Letters* **15**, 6182 (2015).
 - ⁴² N. Marzari, A. A. Mostofi, J. R. Yates, I. Souza, and D. Vanderbilt, *Rev. Mod. Phys.* **84**, 1419 (2012).
 - ⁴³ M. P. L. Sancho, J. M. L. Sancho, and J. Rubio, *Journal of Physics F: Metal Physics* **14**, 1205 (1984).
 - ⁴⁴ R. Yu, X. L. Qi, A. Bernevig, Z. Fang, and X. Dai, *Phys. Rev. B* **84**, 075119 (2011).
 - ⁴⁵ A. A. Soluyanov and D. Vanderbilt, *Phys. Rev. B* **83**, 035108 (2011).
 - ⁴⁶ P. Ghaemi, S. Ryu, and D.-H. Lee, *Phys. Rev. B* **81**, 081403(R) (2010).
 - ⁴⁷ J. Ding, Z. Qiao, W. Feng, Y. Yao, and Q. Niu, *Phys. Rev. B* **84**, 195444 (2011).

- ⁴⁸ D. Xiao, W. Yao, and Q. Niu, *Phys. Rev. Lett.* **99**, 236809 (2007).
- ⁴⁹ E. C. Marino, L. O. Nascimento, V. S. Alves, and C. M. Smith, *Phys. Rev. X* **5**, 011040 (2015).
- ⁵⁰ H. Wang, Q. Niu, and Z. Qiao, *Phys. Rev. B* **104**, 235157 (2021).